322
GEOME 2
Manuscript received: November 7, 2016
Accepted: March 3, 2017

Geologica Macedonica, Vol. **31**, No. 1, pp. 49–65 (2017)
In print: ISSN 0352 – 1206
On line: ISSN 1857 – 8586
UDC: 553.43:528.831.2(55)
Original scientific paper

ASTER SPECTRAL ANALYSIS FOR HOST ROCK ASSOCIATED WITH PORPHYRY COPPER-MOLYBDENUM MINERALIZATION

Hamid Sabbaghi[1], Ali Moradzadeh[1], Hooshang Asadi Haroni[2]

[1]*School of Mining Engineering, College of Engineering, University of Tehran, North Kargar St., Tehran, Iran, 14395-515*
[2]*Centre for Exploration Targeting, Australian Research Council Center of Excellence for Core to Crust Fluid Systems (CCFS), School of Earth and Environment, The University of Western Australia, Crawley, WA 6009*
h.sabbaghi@ut.ac.ir

A b s t r a c t: This study investigates the application of spectral image processing methods to ASTER data for mapping host rock associated with porphyry copper-molybdenum mineralization. The application of remote sensing in identifying variations in surface mineralogy, structural elements, and lithologic contacts can help in identifying such relations. Signatures collected from the Reflection Radiometer (ASTER) data is used to map the host rock of Zafarqand area. The study area is located in the central segment of the Urumieh–Dokhtar Volcanic Belt of Iran. The Urumieh-Dokhtar is a potential zone for exploration of new porphyry copper deposits. Band ratio, Band math, False color composites and Principal component analysis techniques are used to refine the different lithologic units in the area. These methods showed the discrimination of acidic igneous from mediocre igneous and the boundary between igneous rocks using the shortwave infrared bands (SWIR) of ASTER at regional scale. Results have proven to be effective and in accordance with the results of field surveying and ore microscopy examination and with reference geological map. In conclusion, the image processing methods used can provide cost-effective information to discover possible locations of porphyry copper and epithermal gold mineralization prior to detailed and costly ground investigations. The extraction of spectral information from ASTER data can produce comprehensive and accurate information for copper and gold resource investigations around the world, including those yet to be discovered.

Key words: porphyry copper; ASTER; PCA; band ratio; Zafarqand

1. INTRODUCTION

Remote sensing techniques have been widely and successfully used for geological mapping and mineral exploration for decades (Amer et al., 2010; 2012; Zhang et al., 2007). Remote sensing technology plays a vital role in the initial stages of ore deposits exploration especially in arid and semi-arid regions. Recognizing host rocks through remote sensing instruments have been widely and successfully used for the exploration of epithermal gold and porphyry copper deposits (Azizi et al., 2010; Bedini 2011; Pour & Hashim, 2011, 2012b). ASTER data has been used extensively in the last decade for geological mapping and mineral exploration because of the high spectral characteristics and low cost (Aboelkhair et al., 2010; Amer et al., 2010; Azizi et al., 2010; Bedini, 2011; Pour & Hashim, 2011). The six spectral bands of ASTER shortwave infrared radiation subsystem were designed to measure reflected solar radiation to distinguish Al–OH, Fe, Mg–OH, Si–O–H and CO absorption features (Clark et al., 1990; Hunt, 1977; Hunt & Ashley, 1979). Moreover, the ASTER VNIR and TIR data can provide sufficient capability for the remote identification of vegetation and iron oxide minerals in surface soil and the mapping of carbonates and silicates, respectively (Bedell, 2001; Y. Ninomiya, 2003; Rockwell & Hofstra, 2008). Rocks and minerals have higher reflection in shortwave infrared radiation (SWIR) than visible and near infrared radiation (VNIR) wavelength regions. ASTER has six SWIR bands that can give more information and accurate results for lithologi-

cal mapping and mineral exploration. Increasing demand for copper in the global market made it a necessity to prospect for new occurrences in the region through the development of new techniques. The new techniques are particularly useful in regions with extremely rugged topography, where it is impossible to do conventional geological mapping. The 20th century witnessed a huge development in remote sensing sensors as well as its associated image analysis techniques, which minimized the geologist's efforts before and during field expeditions. The newly developed sensors provide detailed information on the mineralogy of different rock types comprising the Earth's surface (Moghtaderi et al., 2007; Zhang et al., 2007). The development of satellite data analysis techniques increases the amount of confidence and accuracy of the investigated targets, especially those related to both lithological and hydrothermal alteration mapping (Gabr et al., 2010; Liu et al., 2007; Rajendran et al., 2013; Zoheir, 2011; Zoheir & Emam, 2012). The earlier studies of this ore deposits type were about detecting their alteration zones and have provoked constant interest to map their host rock. The first step for detecting and discovering and specific ore deposit type is distinguishing host rock and then alteration zone. Porphyry copper and epithermal gold mineralization deposits typically occur in acidic igneous to mediocre igneous such as rhyolite, dacite, diorite and granodiorite, that can be detected by their spectral absorption features. Spectral absorption features are generated by vibrational processes due to over tones and combination tones of fundamental minerals groups (Pour & Hashim, 2012b). Existing at least low of these rocks with together can be good explorative guidance for discovering these deposits type, if also along it, alteration zone can be distinguished.

These rocks are consisted composition of feldspar and plagioclase minerals group, about 60%. Hence, it is very much important to understand the spectral absorption characters of such rocks having similar major mineralogical compositions and interest to distinguish them for better mapping and exploration in remote sensing technique.

The objectives of this research include: 1) To map the host rocks associated with porphyry copper-molybdenum mineralization using combination of band ratio, band math, false color composite and uphold results by principal component analysis (PCA) at regional scale. 2) To discriminate the rhyolite as acidic igneous rock from granodiorite, dacite and diorite as mediocre igneous. 3) To compare the capability of image processing methods used to identify host rock for porphyry copper-molybdenum mineralization. 4) To validate the remote sensing results through comparison with field reconnaissance, microscopicand petrographic analysis and laboratory spectral measurements.

2. GEOLOGICAL SETTING

2.1. *Urumieh–Dokhtar*

The Urumieh–Dokhtar volcanic belt (Central Iranian volcanic belt) trending NW-SE is located in the Tethyan copper belt of Iran. It is the product of Tethys oceanic plate subduction under the Iranian micro-plate followed by continent-to-continent collision of the Arabian and Eurasian plates (Pour & Hashim, 2012b; Regard et al., 2004), which is classified as an Andean volcanic arc (Pour & Hashim, 2012b). In Iran, many of the known and mined porphyry copper deposits are concentrated in this belt, and are particularly widespread in the southeastern belt segment (Shafiei et al., 2009).

In this belt, mountains include a volcanic succession of Eocene calc–alkaline basaltic andesites and Oligocene shoshonitic rocks intruded by Neogene quartz diorites, quartz monzonites and granodiorites, which contain vein type and porphyry copper mineralization. Additional plutonic rocks include granite and gabbro, and volcanic rocks contain basalt, andesite and dacite, which were erupted as lava flows, ignimbrites and pyroclastic flows. The most of volcanism occurred from Eocene to Miocene time in this belt (Pour & Hashim, 2012b).

Extensive mineralization occurred from Miocene to Pliocene time and produced porphyry copper and vein type mineralization. Porphyry copper deposits are associated with Miocene adakitelike orogenic granitoids that intruded the Eocene volcanic rocks (Shafiei et al., 2009). Giant porphyry copper ore deposits in this belt include Sar Cheshmeh in a granodiorite-quartz-monzonite pluton and Meiduk in a quartz diorite pluton (Hezarkhani,

2006). In this area, yearly precipitation averages 25 cm or less (Modarres & Da Silva, 2007), thus the deposit's exposure is well due to sparse or non-existent vegetation cover.

2.2. *Study area*

2.2.1. *Location and condition*

Zafarqand copper-molybdenum deposit is located in northeast of Isfahan province in Iran which is shown in Figure 1. This deposit distances directly 89 km from the center of Isfahan, 22 km from the south of Ardestan and 6 km from the west of Zafarqand village. Tehran-Kooh, Kooh-Chenar and Kooh-Jogand can be named from the most important heights in the study area. The average elevation from the sea is 1800 m and the weather is temperate with cold winters and hot summers. The vegetation is sparse, the average precipitation is low and snow can seldom be observed. From the point of weather, mining activities can be carried out during all the seasons.

Fig. 1. Field photograph showing the Zafarqand copper-molybdenum mineralization area

2.2.2. *Geological background*

The study area includes low heights and foothills and from the tectonic view, it is placed at the edge of Central Iran zone and Urumieh-Dokhtar volcanic belt. The volcanic rocks of the third era are major basement rocks of the study area and also intrusions are placed at the edge. Dacite rocks which are locally converted to rhyodacite and rhyolite, can be observed at the west of the village which include Gazighe mountain. The mentioned parts at the most eastern section are converted to white colored rhyolite and rhyodacite rocks that can be separated readily and the evidences of porphyry system are concentrated in this section.

Tuff and rhyolite-rhyodacite ignimbrites which come back to Eocene-Oligocene are observed at the south and southeast parts of the study area which can be seen on geologic map (Figure 2). Also rhyodacite-rhyolite units and rhyolitic tuffs can be seen at the south and southwestern parts of the village. Marbin-Rangan major fault is the main structure in the study area which strikes from Marbin village to Rangan train station and Abyazan area. It separates two geologic zones of Sanandaj-Sirjanand Urumieh Dokhtar volcanic belt. This fault strike is NW-SE and passes from the southern part of the study area. There is also another fault named Bargowhar which strikes nearly perpendicular to the Marbin-Rangan fault which intersects the study area. There are also several other faults located at the edge of intrusions in Taqi-Abad village which are probably separated from regional tectonic system of the study area and they have been generated mainly by the pressure of intrusions.

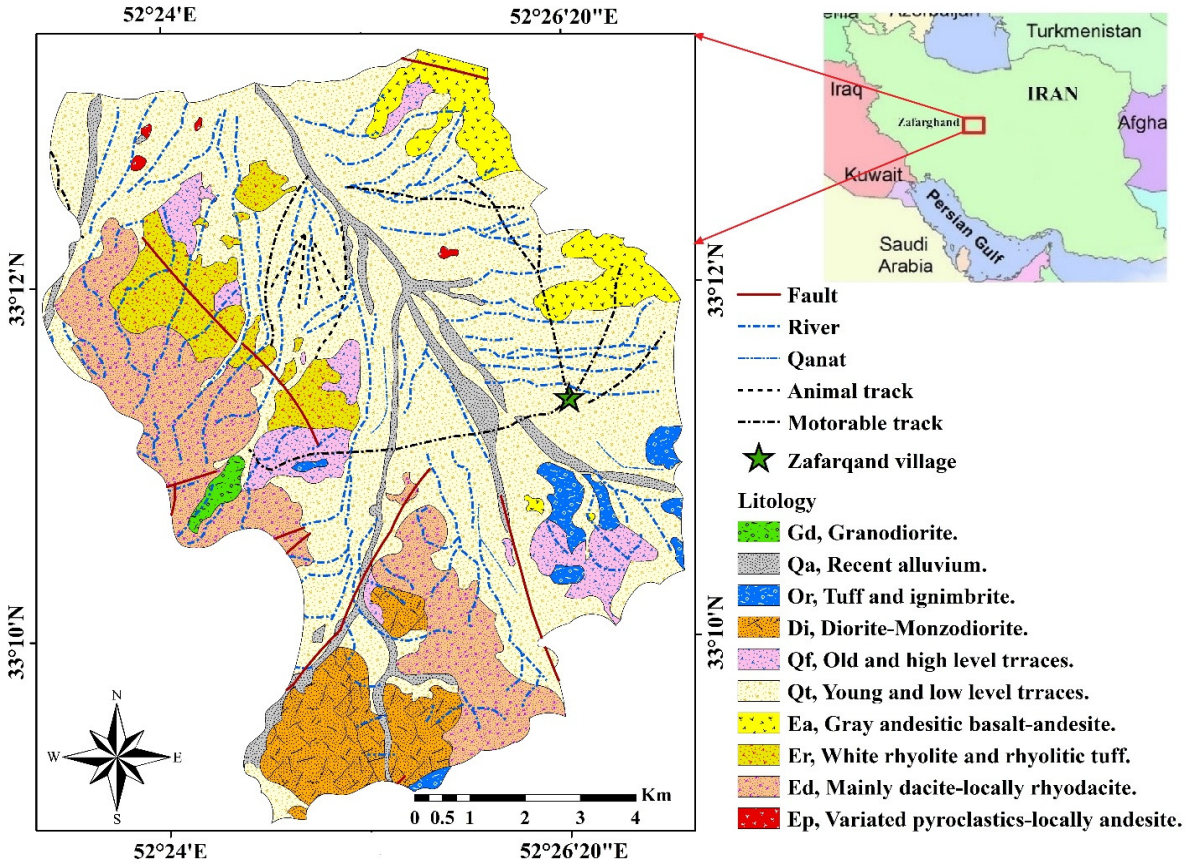

Fig. 2. Geologic map of Zafarqand. The red box is the Zafarqand area

3. MATERIALS

3.1. *ASTER data*

Advanced Spaceborne Thermal Emission and Reflection Radiometer (ASTER) imagery was used to identify host rock of porphyry copper mineralization in the study area. ASTER level-1B data product was obtained from the Land Processes Distributed Active Archive Center at NASA. The ASTER level-1B data are registered radiance at the sensor product contains radiometrically calibrated and geometrically co-registered data for the original ASTER level-1A data (Amer et al., 2016).

3.2. *Reference spectra*

Minerals of earth surface have a unique response in interaction with electromagnetic radiation and creates a diagnostic spectral signature (Gupta, 2003; Rajendran et al., 2013) which conveys unique information related to the particular mineral. Acidic and mediocre igneous rocks are predominantly formed by plagioclase and feldspar minerals group in different proportions, and have a diagnostic spectral absorption feature which can be used to distinguish each other. Rhyolite important constituent minerals are albite, oligoclase (plagioclase) and sanidine (feldspar) (Bachmann & Bergantz, 2004), while the most superabundant minerals in granodiorite are oligoclase (plagioclase), microcline and orthoclase (feldspar) (Wang et al. 2003), also dacite and diorite were contained much amount plagioclase (andesine) and seldom minor amount feldspar (for dacite) (Austin, 1996; Wang et al., 2003).

Reference spectra of these minerals were obtained from the ASTER JPL and USGS spectral libraries. The ASTER spectral libraries provide reflectance spectra of several minerals, most of them are presented at two or more different grain sizes to demonstrate the effect of particle size on reflectance spectra (Amer et al., 2016).

Laboratory spectra of albite, oligoclase, andesine, orthoclase, microcline and sanidine resampled to ASTER band passes. Nearest neighbor resampling method uses the nearest pixel values without any interpolation so it was used to maintain the original pixel values of the image. The absorption features of reflectance spectra of albite, oligoclase, andesine, microcline, orthoclase and sanidine in the range of wavelength between SWIR are given in Figure 3a. Albite and oligoclase display an absorption feature at 2.18 µm that correspond with ASTER band 5 (Figures 3a & 3b), while andesine (mediocre plagioclase) exhibits absorption feature situated at 2.28 µm, which coincide with ASTER band 7 (Figures 3a & 3b). Orthoclase, microcline and sanidine, which all present absorption feature centered at 2.22 µm, coinciding with ASTER band 6 (Figures 3a & 3b).

Based on the spectral absorption characters of such minerals, the minerals bearing rock types are discriminated using several image processing methods including band ratio, band math, false color composites and principal component analysis by ASTER SWIR band, especially bands 5, 6 and 7. According to Rajendran et al. (2013), also some silicate minerals display absorption feature at 1.6–1.7 µm (ASTER band 4). Moreover, these rocks were contained little content of biotite and hornblende (amphibole), about 10% that both have absorption feature at 2.3 µm (ASTER band 8) (Rowan et al., 2005).

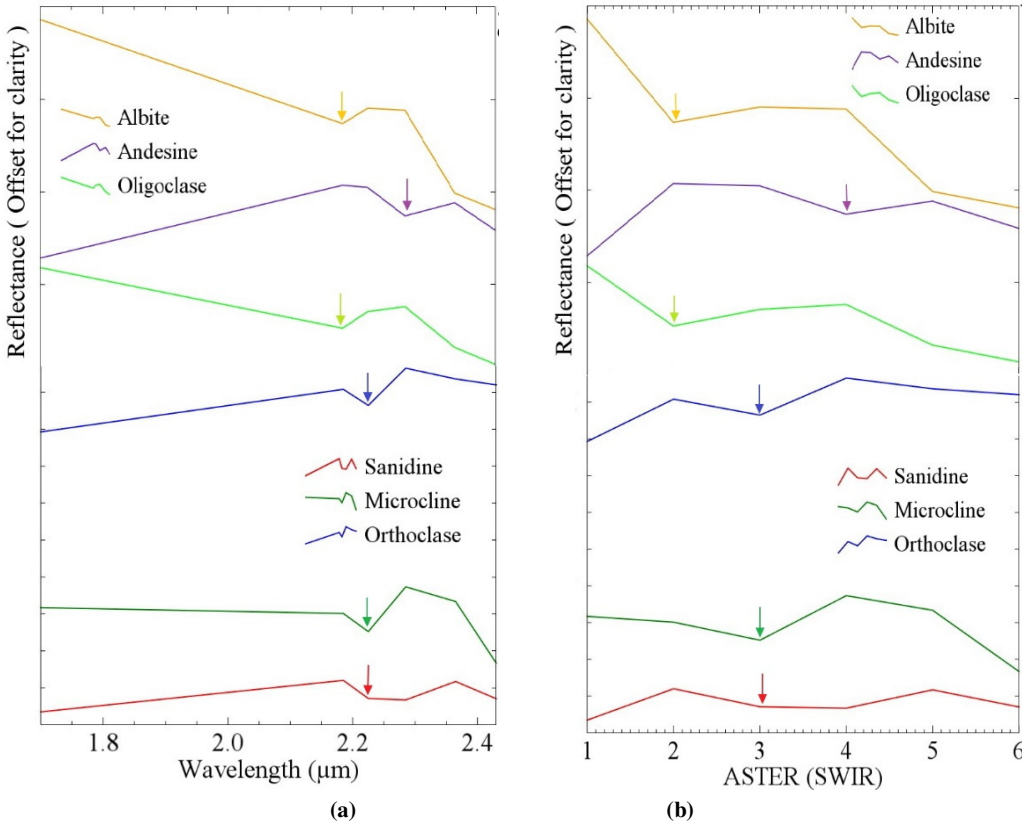

Fig. 3. Laboratory spectra of feldspar and plagioclase minerals group |(**a**) based on wavelength, (**b**) based on band number

3.3. *Field work*

Field work encompassed sampling of fresh host rocks and quartz veins (Figures 4a & 4b). Field mapping was conducted to verify the contacts between the lithological units and structural patterns. Systematic field works were carried out at several locations. Ore samples were collected from the hydrothermally altered and fresh host rocks (Figures 4c–4e) from near surface and subsurface at Zafarqand area by ANJ Company. The samples are used for spectral measurements, megascopic, microscopic, and minerals studies at the laboratory of Aflak Exploration Company.

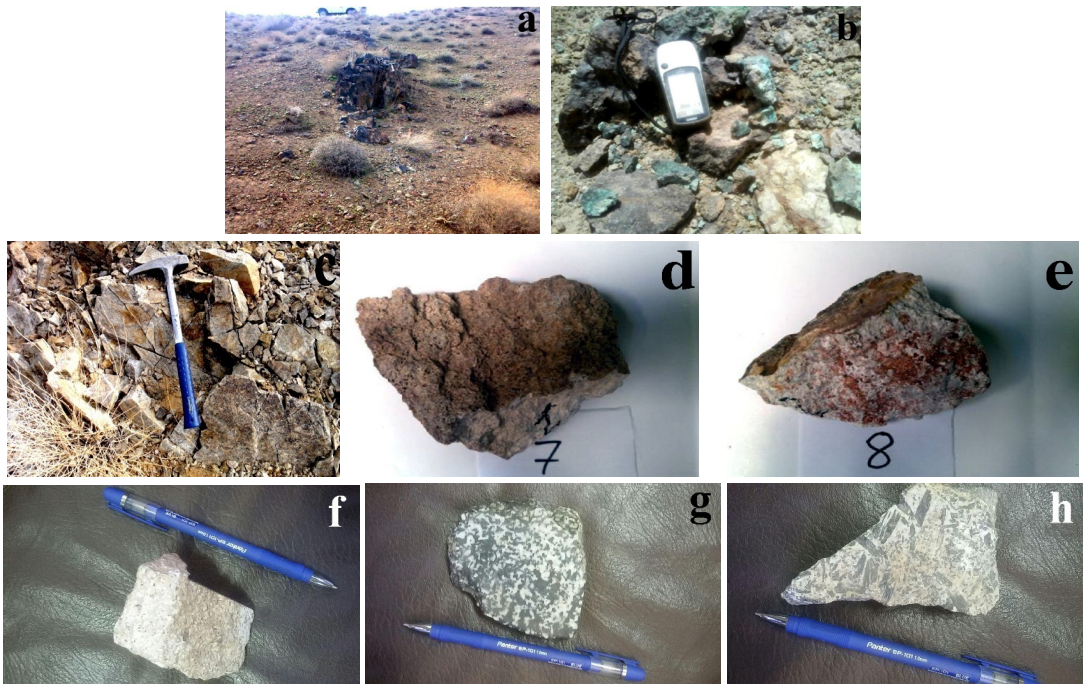

Fig. 4. (**a**) Far view of silica veins consist of copper mineralization in granodiorite rock with extreme potassic alteration. **(b)** Near view of silica veins consist of malachite mineralization (dacite rock) in Zafarqand porphyry copper-molybdenum index. **(c)** Near view of diorite rocks with extreme potassic alteration. **(d)** & **(e)** Hand samples of dacite porphyry with extreme phyllic alteration. **(f)** Hand-specimen of rhyolite. **(g)** & **(h)** Hand-specimens of diorite

3.4. *Laboratory studies*

The spectral properties of samples were studied by measuring the spectrum using a PIMA SP infrared spectrometer instrument which is fabricated for field spectroscopy by Integrated Spectronics Pty Ltd., Australia. It identifies and analyzes the spectral signal of minerals in the wavelength ranges from 1300 to 2500 nm with PIMA VIEW software (version 3.1). The spectral resolution of the device is about 7 nm. It has a built in wavelength calibration target plate and is capable to measure spectra from 10 s to around 5 min speed. spectral measurements have been taken using a PIMA SP infrared spectrometer at different locations in the field and over the samples collected in the laboratory. The obtained spectral plots over the samples are well correlatable with the studied spectra. That spectral plots of selected samples of rhyolite, granodiorite, dacite and diorite are given in Figure 5. The spectra of these rocks collected over the samples in the laboratory show noisy due to the streaky surface of samples.

The rhyolite spectral plots show the spectral absorptions around 1.8 (band 5) µm due to the absorption of albite and oligoclase, also at around 2.2 µm (band 6) (Fig. 5a) due to the absorption of sanidine. Granodiorite display absorption features at 1.8 µm that belongs to oligoclase and 2.2 µm due to the absorption of orthoclase and microcline (Figure 5b), eventually dacite and diorite present absorption features at 2.28 µm (band 7) due to much content of plagioclase (andesine) (Figures 5c & 5d).

The study on the intensity of the total absorptions against the reflections of these rocks in reflectance value axes shows the variations in intensity of absorptions. These are due to the variations in mineral compositions occurred in the surface of the rocks, which can be considered as an important reflectance parameters to distinguish these rocks and discriminate them in SWIR regions. The rhyolite and granodiorite (Figures 5a & 5b) show the intensity of total absorptions differences between 50 and 90% and 30 and 70%, respectively, whereas the dacite and diorite (Figures 5c & 5d) show intensity differences between 10 and 60% and 5 and 50%, respectively. The low intensities of absorptions (and high reflection values) of rhyolite and granodiorite compare to the high intensity of absorptions (and low reflection values) of dacite and diorite are due to the presence of SiO_2 content that occurred in different proportions in these rocks (Bachmann & Bergantz, 2004; Streckeisen, 1979; Wang et al., 2003).

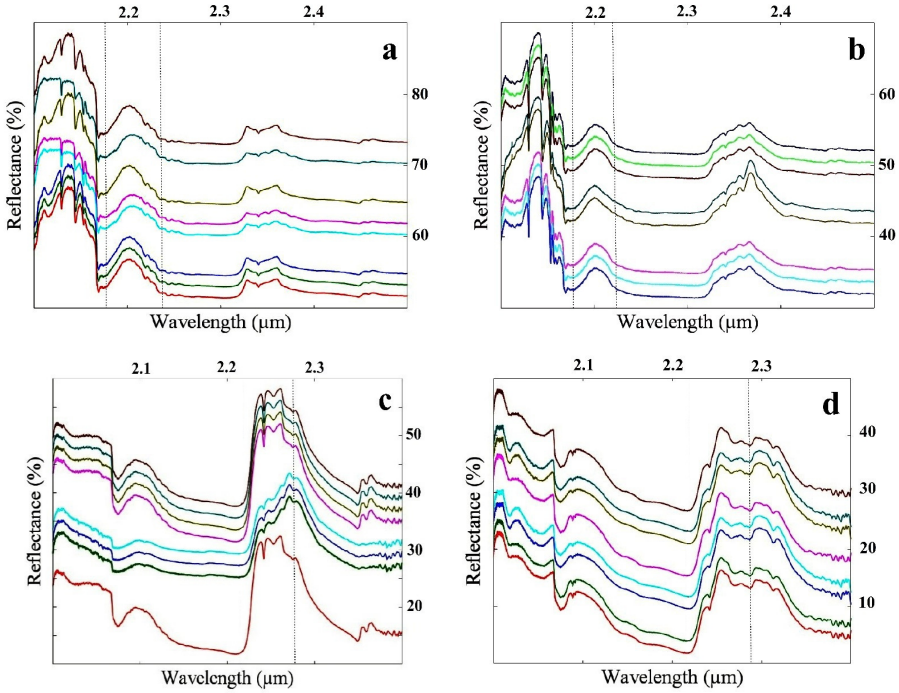

Fig. 5. Laboratory spectral plots of igneous rocks
(a) rhyolite samples, **(b)** granodiorite samples, **(c)** dacite samples, **(d)** diorite samples

4. METHODS

4.1. *Image pre-processing*

An ASTER level-1B image covering the study area was acquired on March 26, 2006, and processed using ENVI 5.3 software from Excel is Visual Information Solutions and Arc GIS 10.2 from Environmental Systems Research Institute (ESRI). These have been evaluated by field checking and laboratory studies. The regional geological maps were used to verify the processed remote sensing data and occurrences of such igneous rocks in field.

Radiometric correction is essential for ensuring high-quality information from remote sensors. The ASTER SWIR data may be affected by the 'crosstalk' instrument problem, which is an offset or additive error in radiance due to the leakage of photons from one detector element to another. This cross detector leakage is most pronounced from band 4 to bands 5 and 9, but it also affects all SWIR bands (Alimohammadi et al., 2015). For very dark pixels adjacent to bright pixels, the crosstalk effect will approach 100% of the input radiance signal (Alimohammadi et al., 2015).

The path radiance effect was minimized by using the Dark Subtraction method and the solar radiation response (Abrams, 2002). The ASTER imagery was radiometrically corrected for retrieving spectral reflectance using ENVI automated module Quick Atmospheric Correction (QUAC), and Cross-track illumination correction (Amer et al., 2016).

4.2. *Image processing*

4.2.1. *False-color composite (FCC)*

The false-color composite (FFC) image can be produced by merging visible and infrared bands or by using infrared bands only. The interpretation of FCC images depends on how these bands are assigned to the three principal colors – red-green-blue (RGB), used for the image display which in turn depend on the spectral characteristics of rocks and minerals (Ibrahim et al., 2016).

4.2.2. *Band ratio and band math*

Band rationing is a very simple and powerful remote sensing technique, in which the digital number (DN) values of one band are divided by the corresponding (DN) values of another band. This technique emphasizes the anomalies of the target objects and enhances the spectral differences between surface materials that are not detected in

either of band images independently (B Zoheir & Emam, 2014).

Band ratio images designed to display the spectral contrast of specific absorption features have been used extensively in geologic remote sensing (Cudahy et al., 2008; Di Tommaso & Rubinstein, 2007; Mars & Rowan, 2006). Band ratios are very useful for highlighting certain features or materials that cannot be seen in the raw bands. The use of mineralogical indices from ASTER band ratios is found efficient for lithological and hydrothermal alteration discrimination (Aboelkhair et al., 2010; Di Tommaso & Rubinstein, 2007; Khan & Mahmoud, 2008; N. Ninomiya et al., 2005; Y. Ninomiya, 2003; Zhang et al., 2007;. Velosky et al., 2003) distinguished the propylitic alteration zone and goss an associated with massive sulfide mineralization in host rocks by using ASTER (4/2, 4/5, 5/6) band ratio images. The ASTER band ratios (4/7, 4/1, 2/3, 4/3) and (4/7, 3/4, 2/1) images were used by Abdeen et al. (2001) for mapping of ophiolites, metasediments, volcaniclastics and granitoids lithological units of the Neoproterozoic Allaqi Suture of the southern Eastern Desert of Egypt. (Amer et al., 2010) constructed the ASTER band ratios ((2 + 4)/3, (5 + 7)/6, (7 + 9)/8) by summing the bands representing the shoulders of absorption features as a numerator, and the band located nearest the absorption feature as a denominator to discriminate different ophiolitic and granitic rocks in a red–green–blue (RGB) color combination and identified the ophiolitic rocks, metagabbros and metabasalts.

ASTER band ratios are more effective in characterizing certain rocks and minerals, and also can discriminate acidic igneous of mediocreigneous in terms of their improved spectral bands in SWIR region and spatial resolution. Yamaguchi & Naito (2003) proposed several spectral indices for lithological discrimination and mapping of exposed surface rock types using ASTER shortwave length infrared (SWIR) bands.

Based on resumed results from references spectra and laboratory studies, bands 4, 5, 6 and 7 for discriminating studied igneous rocks are so important, therefore these bands were applied more than other bands in band ratio and band math processings.

The resulting RGB indices are listed as follows:

$$\text{Rhyolite index (RHI)} = \left[\frac{\text{band 6}}{\text{band 5}}\right]\left[\frac{\text{band 6}}{\text{band 8}}\right]\left[\frac{\text{band 6}}{\text{band 9}}\right] \quad (1)$$

$$\text{Dacite index (DAI)} = \left[\frac{\text{band 5}}{\text{band 7}}\right]\left[\frac{\text{band 4}}{\text{band 6}}\right][\text{band 4} + \text{band 8}] \quad (2)$$

$$\text{Diorite index (DII)} = \left[\frac{\text{band 5}}{\text{band 7}}\right]\left[\frac{\text{band 4}}{\text{band 6}}\right][\text{band 4} + \text{band 6}] \quad (3)$$

$$\text{Granodiorite index (GDI)} = [\text{band 4} + \text{band 0}]\left[\frac{\text{band 6}}{\text{band 8}}\right]\left[\frac{\text{band 5}}{\text{band 8}}\right] \quad (4)$$

4.2.3. *Principal component analysis*

Crosta et al., 2003 used Principal Component Analysis (PCA) on ASTER VNIR and SWIR bands in order to target key alteration minerals associated with epithermal gold deposits in Los Menucos, Patagonia and Argentina. PCA technique can extract detailed mineralogical spectral information from ASTER data by producing abundance images of selected minerals (Pour & Hashim, 2012a).

Principal component analysis (PCA) is a multivariate statistical technique that selects uncorrelated linear combinations (eigen vector loadings) of variables in such a way that each successively extracted linear combination, or principal component (PC), has a smaller variance (Abrams et al., 2002; Zoheir & Emam, 2014).

Image enhancement technique PCA transform have been implemented on the calibrated SWIR spectral bands of the ASTER image. This image enhancement technique are also called as spectral data reduction as that reduce the spectral redundancy of the image. The PCA transform is a important multivariate statistical technique and used to produce uncorrelated output bands, to segregate noise components and to reduce the spectral dimensionality of the data in a such a way that the first PC band contains a high variance or eigen value, the second PC band contains second high variance and the last PC band contains the minimum variance, high correlation and noise (Kumar et al., 2015; Zoheir & Emam, 2014), hence PCA transform helps to enhance and separate spectral signatures from the background (Gabr et al., 2010).

PCA was applied touphold band ratio and band math results with selected subsets of six ASTER bands according to the position of characteristic spectral absorption features of note worthy igneous rock in the SWIR regions. PCA outputs are presented as tables of statistic factors and selected PCA images from these transformations are reproduced in figures to support the discussion. False color composite was assigned to considerable

PCA images to visualize the results. The image eigen vectors and eigen values obtained from PCA using covariance matrix on six SWIR bands. The statistic results derived from principal components transformation to SWIR bands of ASTER are shown in Table 1.

The statistic results of PCA for SWIR bands indicate that the first principal component (PCA1) is composed of a positive weighting of all total bands and has 98.32% (eigen value) of the spectral information (Table 1). Considering the eigen vector loadings in PCA2 to enhance igneous rocks in bands 5, 6 and 7 (Table 1), it is evident that igneous rocks manifest as bright pixels in PCA2 because of the positive contribution from band 6 (0.7707), and negative contribution from band 5 (–0.469) and band 7 (–0.339). PCA3 distinguishes igneous rocks by bands 5, 6 and 8 (Table 1), hence igneous rocks differentiated as dark pixels in this PCA because of the negative contribution from band 5 (–0.583), and positive contribution from band 6 (0.535) and band 8 (0.413).

PCA4 has great negative contribution in band 7 (–0.654), positive contribution in band 9 (0.682) and also small negative contribution in band 5 (–0.2). Therefore, PCA4 discriminates igneous rocks as dark pixel from the background consists of other rock types (Table 1). PCA5 and PCA6 are noisy.

T a b l e 1

Principal components analysis on SWIR bands of ASTER, Ardestan scene.

Eigen vectors	Band 4	Band 5	Band 6	Band 7	Band 8	Band 9	Eigen values (%)
PC 1	0.50326	0.45915	0.41649	0.39196	0.35055	0.29309	**98.32**
PC 2	–0.2612	**–0.46908**	**0.77075**	**–0.33952**	–0.0488	0.00206	1.11
PC 3	–0.3309	**–0.58387**	**0.53575**	–0.2487	**0.4135**	0.17228	0.28
PC 4	0.17860	**–0.2002**	–0.015	**–0.6540**	0.18432	**0.6826**	0.13
PC 5	–0.0582	–0.6466	0.74358	0.13042	–0.0917	–0.00828	0.07
PC 6	–0.0885	0.20361	0.31995	–0.5210	0.5232	–0.55049	0.06

4.3. *Petrography*

Thirty-six polished thin sections of quartz veins and associated alteration zones within rhyolites, dacite rocks, diorite rocks and granodiorites were studied microscopically and using Scanning Electron Microscope (SEM). Cambridge MK-5 Electron Microscope at 25 kV was employed to study the homogeneity of the sulphides and the heterogeneity of telluride phases.

Petrographic analyses of the rocks were carried out to identify constituent minerals and also to estimate the relative abundance of these minerals based on modal analysis. The copper mineralized is associated with host rocks hydrothermal alteration zones. Altered host rock are controlled by the type of host rock, nature of the mineralizing fluid and style of deformation of host rocks (Amer et al., 2016). In the study area, the hydrothermal alteration minerals display distinct spatial zonation around the quartz veins in metadacites, metadiorites, metarhyolites and even geranodiorites. Petrographically, they consist of feldspar, plagioclase, quartz, biotite, hornblende, sericite, epidot, chlorite, malachite, hematite and iron oxide (e.g. goethite). However, these minerals are not recorded in each examined samples and they occur differentially in the studied samples.

White milky quartz occur as secondary mineral and is found filling amygdals due to silicatization. Quartz is the most common gangue mineral in porphyry copper-molybdenum host rock. Coarse quartz crystals called magacryst that some of them are affected by the silica metal and faced chemical corrosion in gulf form (Figures 6a & 6b). Sericite (fine-grained variety of muscovite) occurs either as euhedral to subhedral disoriented crystals commonly developed as a result of hydration of plagioclase. Plagioclase (oligoclase, andesine or albite) and orthoclase minerals can be altered as far as the surface of them shows kaolinite and sericite, and it causes lack of observing them completely. Clay minerals contain many fine, highly birefringent shreds (presumably kaolinite or alunite) and they are randomly distributed and closely associated with quartz and sericite. They are mostly produced as intracrystal voids filled by hydrothermal solutions (Figures 6c & 6d).

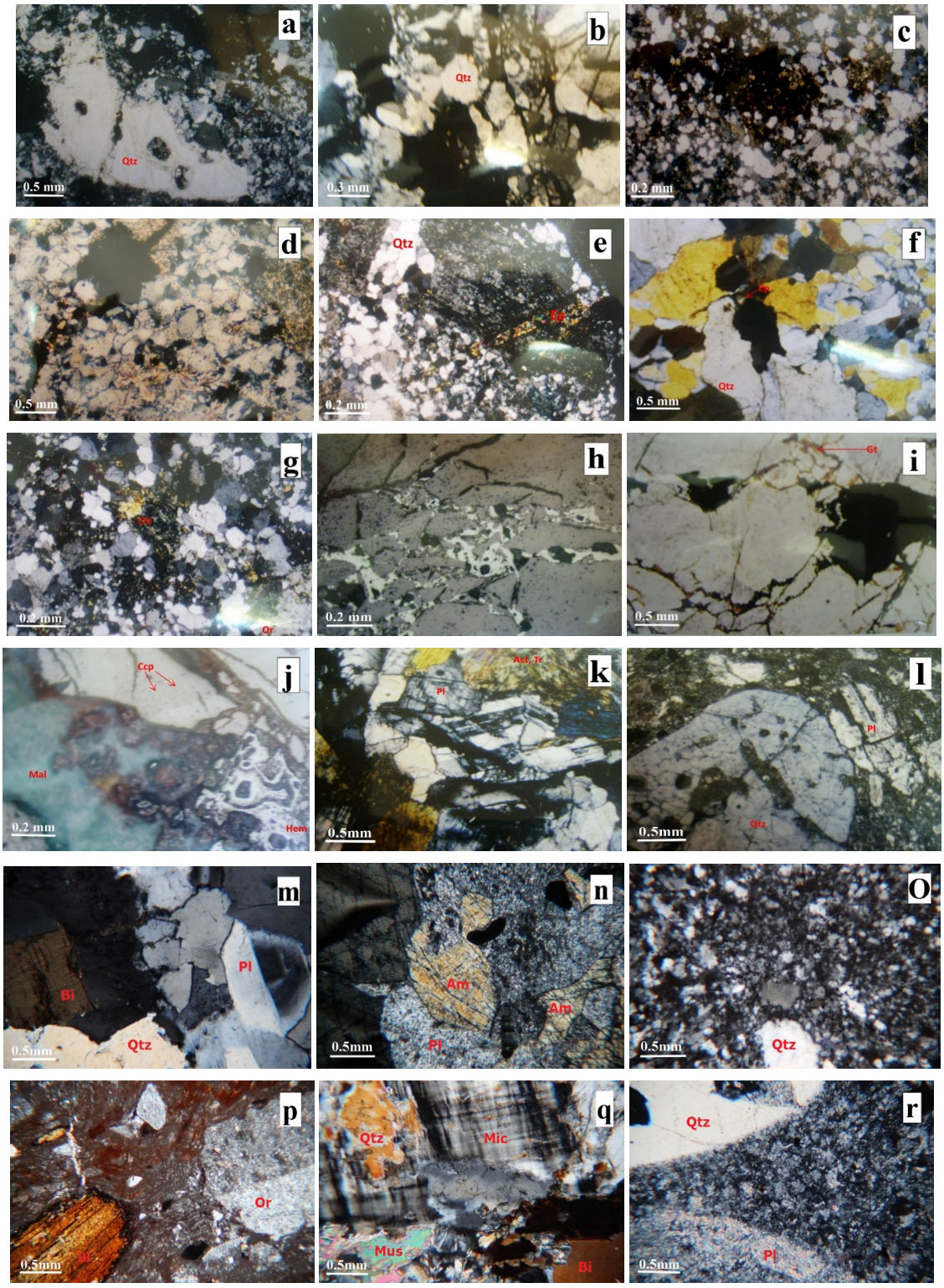

Fig. 6. **(a)** Megacryst of quartz in rhyolite rock that shows gulf corrosion among fine crystals of quartz and sericitized feldspars (point 7). **(b)** The concentration of fine and coarse quartz minerals that shows deformation phenomenon and the fractures which are filled by hematite in rhyolite. **(c)** Feldspar sericitization and the formation of sericite and epidote among quartz crystals in the dacite rock (point 2). **(d)** Sericitized feldspars in the right section of the figure and sericite crusts among the quartz crystals and vein of iron oxide can be seen in the granodiorite rock. **(e)** The formation of epidote mineral with vein and granular texture in diorite rock which has been intersected by quartz vein (point 10). **(f)** Quartz vein with 0.5 cm thickness and the formation of ore at the center of vein along with the formation of epidote in granodiorite. **(g)** Fine crystals of

chlorite along with inter-granular epidote in granodiorite rock; also sericitized orthoclase in lower part of the section can be observed. (**h**) The concentration of hematite along the veins and fractures in the mettle of plagioclase (andesine) in dacite rock (point 9). (**i**) Fractures and veins in dacite rock which are filled by hematite and goethite (point 8). (**j**) Hematite minerals with colomorph texture in the surrounding parts of goethite, and a mass of malachite along with two small crystals of chalcopyrite in dacite rock can be seen in the figure (point 1). (**k**) Granuler texture in diorite rock with mediocre plagioclase crystals (andesine) and tremolite-actinolite mineral (point 12). (**l**) Quartz with gulf corrosion and acidic plagioclase (albite) with polysynthetique macle in rhyolite rock (point 6). (**m**) Quartz crystal with plagioclase (oligoclase) mineral with polysynthetique macle and zoning, also biotite in granodiorite rock (point 4). (**n**) Alterated plagioclase (andesine) and amphibole (hornblende) in diorite rock (point 11). (**o**) Quartz mineral in background of plagioclase and feldspar in rhyolite rock. (**p**) Rhyolite section shows feldspar (orthoclase) and biotite minerals in mettle of sanidine and orthoclase with minor amount glass (point 5). (**q**) Muscovite mineral at left edge of section with feldspar (microcline), quartz and biotite in granodiorite rock (point 3). (**r**) Sericitized plagioclase and quartz with gulf corrosion in rhyolite rock.

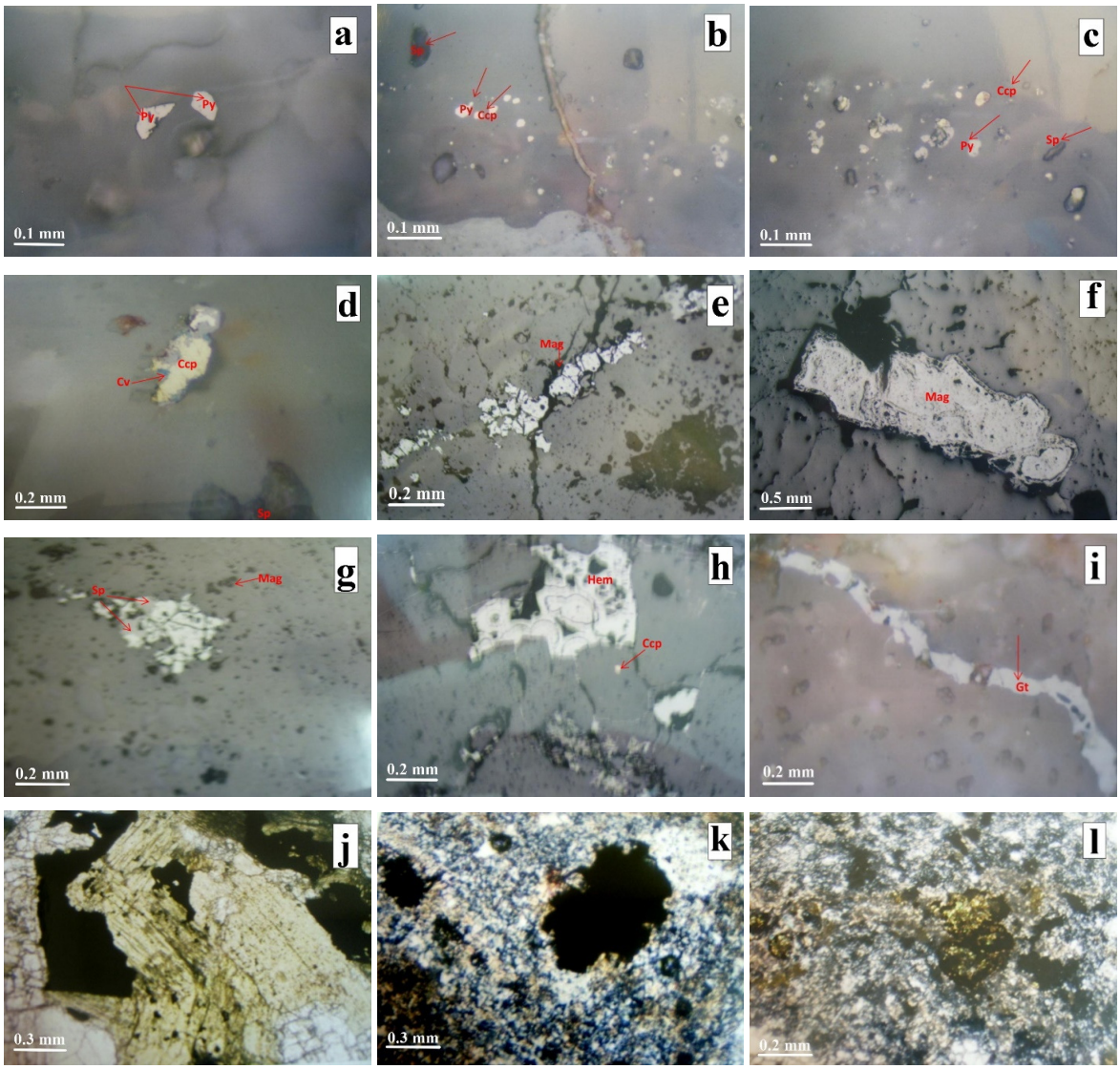

Fig. 7. (**a**) Small and semi-crystalline pyrite crystal in rhyolite rock (point 5). (**b**) Hexahedron nature of pyrite and amorphous granules of chalcopyrite in rhyolite rock which can be observed clearly (point 6). (**c**) Small and dispersed granules of chalcopyrite in relation with sphalerite and bornite in rhyolite rock (point 7). (**d**) Chalcopyrite in dacite rock which has been altered at the edges and changed to covellite; and also concentration of pyrite at the center of sphalerite (point 9). (**e**) The concentration of amorphous and fine grains of magnetite along the vein in dacite rock (point 8). (**f**) Semi-crystalline magnetite which has changed to goethite in surrounding parts (dacite rock) (point 2). (**g**) Amorphous crystals of magnetite in relation with sphalerite in diorite rock can be seen clearly (point 11). (**h**) Chalcopyrite crystal and colomorph texture in hematite mineral in diorite rock (point 12). (**i**) Vein of goethite in rhyolite rock. (**j**) The concentration of ore among the tremolite-actinolite and plagioclase crystals of diorite rock (point 10). (**k**) The concentration of ore at the granodiorite rock with sericite at the edge (point 3). (**l**) The concentration of ore with iron oxide composition at the surrounding parts of the epidote mineral in granodiorite rock (point 4)

Calcium-rich solutions cause the formation of epidote with granular and inter-granular textures, and also veins along with silica in the diorite rock that changes into chlorite by alteration (Figures 6e–6g). Hematite which shows the forming of ore after the rock formation in typical tectonic conditions, is placed along the veins and fractures (Figures 6h–6j). Quartz, feldspar, plagioclase, biotite and hornblende phenocrysts are observed in mettle of plagioclase and feldspar in igneous rocks (Figures 6k–6r).

4.3.1. *Ore petrography*

Microscopic analysis of the ore samples identified pyrite, chalcopyrite, pyrrhotite, sphalerite, magnetite, covellite and iron oxides minerals. Pyrite is the most abundant and occurs as subhedral and euhedral grains, included in quartz and shares the boundaries with chalcopyrite. Chalcopyrite is mostly amorphous while pyrite is crystalline (Figures 7a–7d). Pyrrhotite mostly occurs as intergrown crystals with sphalerite and chalcopyrite. Chalcopyrite occurs as intergrown crystals within pyrite and sphalerite (Figure 7d). Occasionally, it replaces pyrite forming wedge-like shape. From the viewpoint of crystallization order, magnetite is formed at first. After the formation of silica veins; pyrite, chalcopyrite, bornite and then sphalerite are formed. Crystalline and semi-crystalline magnetite mineral has changed to goethite mineral in surrounding parts (Figures 7e–7g). Iron oxides (hematite and goethite) are found in oxidizing zones (Figures 7h & 7i). Cu occur as very fine inclusions in tremolite-actinolite, sericite, clay mineral sand epidote (Figures 7j–7l).

5. RESULTS AND DISCUSSION

Combination of the band ratio, band math, principal component analysis (PCA) and false color composite techniques are used in this study for mapping the structural features in the Zafarqand area and surroundings.

Figure 8 displays the results of driving RHI as RGB color composite, that represents rhyolite rocks by blue color. RGB color composite of DAI shows dacite rocks as pink color (Figure 9). Diorite rocks are manifested as yellow color at driving DII (Figure 10). FCC of GDI represents granodiorite rocks as brownish red color (Figure 11). It is evident that this method can detect the boundary between igneous rocks clearly. In this way, GDI showed the boundary between studied igneous rocks and also between other rock types and igneouses, which is more recognizable than other indices in the images.

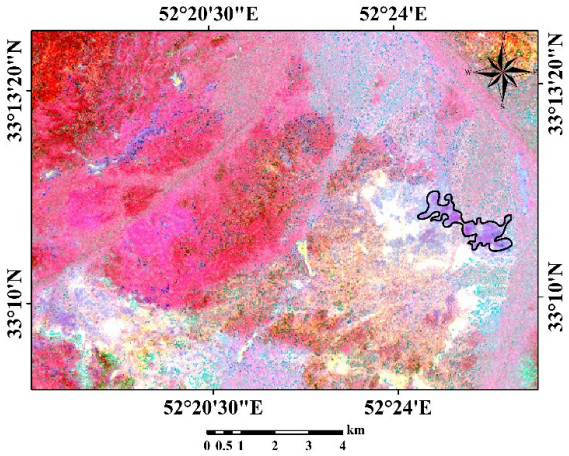

Fig. 8. RGB image of RHI shows rhyolite rock blue color

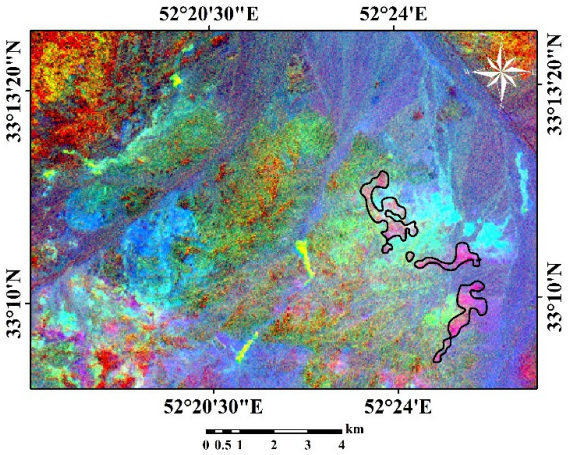

Fig. 9. RGB image of DAI shows dacite rock as pink color

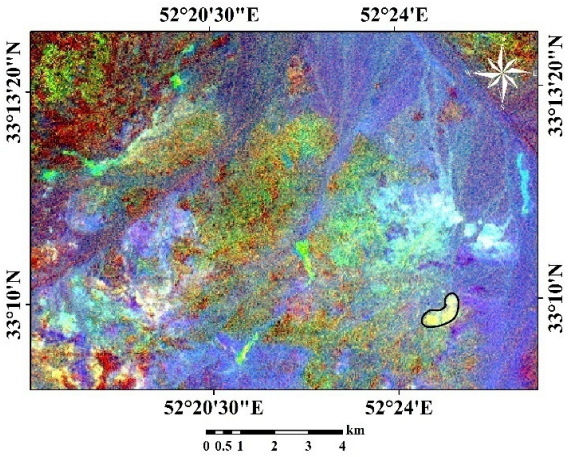

Fig. 10. RGB image of DII shows diorite rock as yellow color

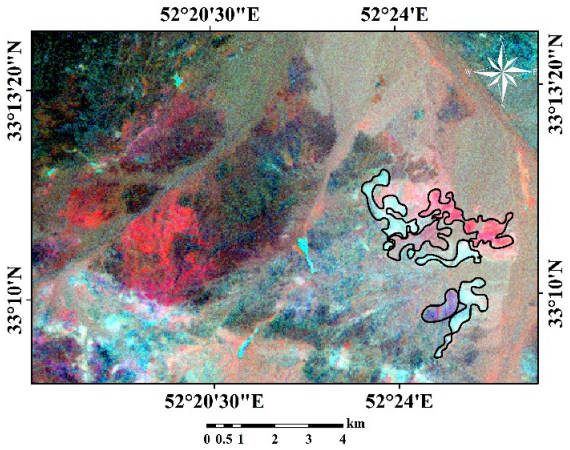

Fig. 11. RGB image of GDI shows granodiorite rock as brownish red color, also distinguishes rhyolite as orange red color, dacite as bluish green color and diorite as dark blue color

These indices provided accurate spectral information for porphyry copper-molybdenum host rock, and lithological mapping, while showing the spatial distribution of these structures well. Also, the resulting maps yielded excellent spatial coherency and strong correlations to published geologic maps of the study areas (Figure 2).

Comparing results of driving indices as RGB to geology map, also to microscopic analysis of collected samples of several locations from study area, evidences to creating and performing these indices successfully. In fact results of references spectra and laboratory analysis denoted bands 5, 6 and 7 as the most important ASTER SWIR bands in discriminating some igneous rocks, that they were applied subtle for creating indices by band ratio and band math. Location of some used samples for microscopic studies has been delineated for conformity on obtained map from GDI index (Figure 12).

Points 1 (Figure 6j), 2 (Figure 6c), 8 (Figure 6i) and 9 (Figure 6h) were dacite rock, these points have situated in dacite zone, that this zone was as bluish green color, points 3 (Figure 6q) and 4 (Figure 6m) were granodiorite and attend in granodiorite zone, points 5 (Figure 6p), 6 (Figure 6l) and 7 (Figure 6a) were rhyolite rock and are in the rhyolite zone, also points 10 (Figure 6e), 11 (Figure 6n) and 12 (Figure 6k) were diorite rock that have situated in diorite zone (Figure 12).

Identification of pelagioclase, feldspar, quartz, biotite and hornblende (index minerals of note worthy igneous rocks) with altered minerals chlorite, epidot and sericite, and also clay minerals from petrographic analyses of the collected hand specimens from the host rock proved that the obtained indices of band ratio and band math techniques (ASTER imagery) using JPL and USGS references spectra was successful in identifying the host rock associated with copper-molybdenum mineralization.

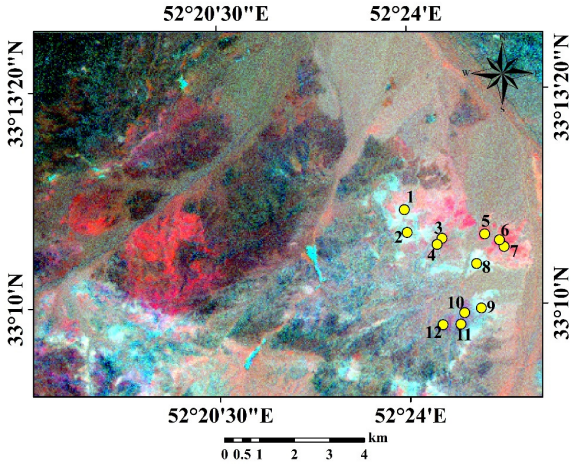

Fig. 12. Location of some collected samples for microscopic studies

The PCA transformation is carried out for the 6 ASTER SWIR bands covering the study area (Zoheir & Emam, 2014). It is generally accepted that the first three high order principal components (1, 2, and 3) can provide over 99% of the spectral information for identifying mineral and rock types that are spatially dominant in the image (Amer et al., 2010). In this study, results from band ratio and band math were repeated and investigated by principal component analysis. Therefore PCA images were drived as RGB color composite based on information of their content, also their results are compared to achieved results from band ratio and band math.

Accordingly, a RGB color composite was produced for PCA1, PCA2 and PCA6 of the Ardestan scene (Fig. 13), show rhyolite rocks as yellow color. It seems that dacite rocks are identifiable as bluish green color at FCC for PCA2, PCA3, PCA6 (Figure 14). RGB color composite of PCA1, PCA5 and PCA6 images show diorite rocks as dark purple color (Figure 15). False color composite of PCA1, PCA3, PCA4 images represent granodiorite rocks as purplish red color (Figure 16). Principal component analyses (PC1, PC3 and PC4) RGB images are powerful in discriminating and unique in interpreting the various igneous rock units in the study region.

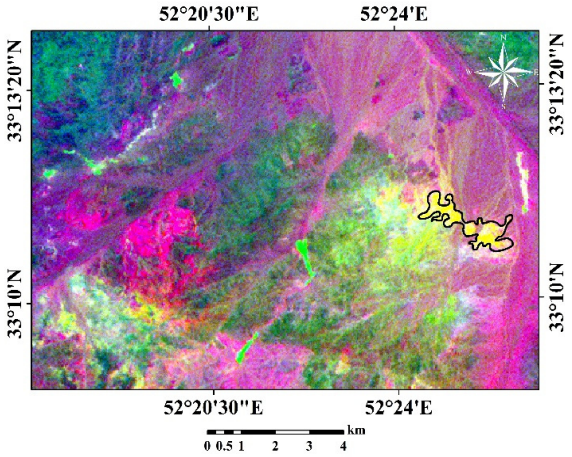

Fig. 13. RGB color composite of PCA1, PCA2 and PCA6 images show rhyolite as yellow color

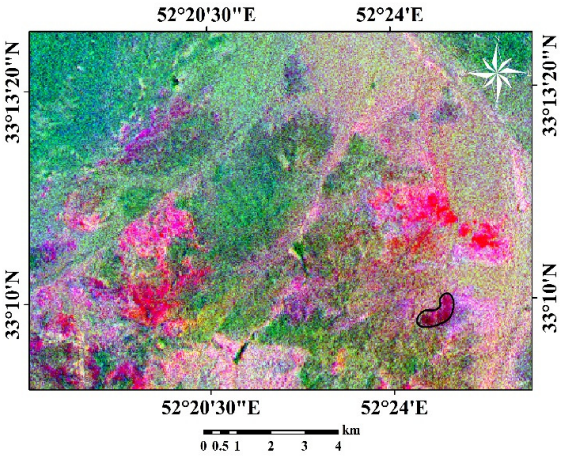

Fig. 15. RGB color composite of PCA1, PCA5 and PCA6 images show diorite as dark purple

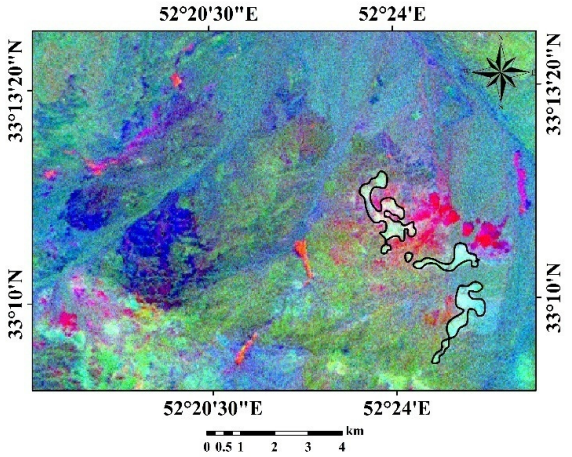

Fig. 14. RGB color composite of PCA2, PCA3 and PCA6 images show dacite as bluish green color

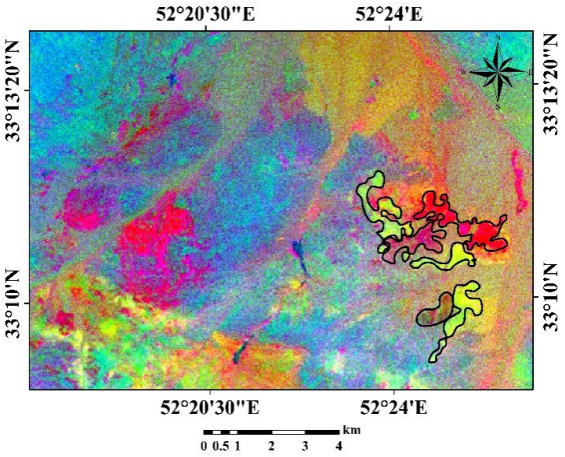

Fig. 16. RGB color composite of PCA1, PCA3 and PCA4 images show granodioriteas purplish red color, also discriminate rhyolite as red color, dacite as light green color and diorite as brownish green color

It is clearly, principal component analysis has investigated results from driving created indices by band ratio and band math as more variety with different colors, these results were cleared especially after comparison Figures 8–11 to Figures 13–16. For example, obtained map from GDI index distinguishes rhyolite as orangish red, granodiorite as brownish red, dacite rock as bluish green and diorite rock as dark blue, while obtained map from RGB color composite of PC1, PC3, PC4 images recognizes them as red color, purplish red, light green and brownish green respectively. In fact performing RGB color composite from PCA images and compare to results of driving indices can avoid of mistakes in discern these rocks.

6. CONCLUSION

The use of ASTER data in mineral exploration and lithological mapping has been increased in recent years due to: (i) spectral characteristics of the unique integral bands of ASTER, which are highly sensitive to important minerals especially in short wave length infrared radiation region; (ii) the possibility of applying several image processing techniques; (iii) 'on-demand' data product availability with low cost (~$60 US or Yen equivalent); and (iv) broad 60×60 km scene coverage useful for

regional scale mapping. It is this enhanced spectral resolution of ASTER in the SWIR wave lengths that allows for reconnaissance mineral exploration from a spaceborne platform.

The present study describes and demonstrates the spectral absorption characters of important host rocks of copper-molybdenum mineralization occurred in parts of the Urumieh-Dokhtar (Zafarqand) studying their laboratory spectral plot and also interpretation of their significant minerals spectra library collected over ASTER satellite data. The spectral absorption of basic minerals from rhyolite, dacite, diorite and granodiorite described in ASTER SWIR spectral bands and demonstrated by studying the image processing methods. These have been verified in the field and studied in the laboratory. The study is time and cost-effective and the outcome may be useful to geologists and exploration communities looking igneous rocks exploration. The technique is proved to be useful in the area of extremely rugged topography in the arid region, where there is difficulty in exhaustive sampling and conventional geological mapping. The RGB color composite image of granodiorite index (GDI) showed well the occurrence of granodiorite and differentiated the presence of other igneous rocks. The PCA1, PCA3, PCA4 RGB image discriminated the acidic and mediocre igneous rocks areas and differentiated the associated lithology, or to other statement, it repeats and investigates veracity and accuracy of GDI index.

Microscopic examination of thin sections shows that the igneous rocks minerals consist es sentially of feldspar, plagioclase, biotite and hornblende that were altered to sericite, chlorite, epidot and clay minerals. The igneous rocks zones of the study area were mapped successfully from the ASTER imagery using the ASTER USGS and JPL references spectra library of their basic minerals. This study suggests more collecting field reflectance spectra of these rocks and laboratory spectral measurements of field samples.

These appropriate image processing methods can provide a reliable, simple, robust, very low cost and user-friendly approach for exploration geologists to identify host rocks assemblages associated with porphyry copper especially copper-molybdenum type and also epithermal gold mineralization, hence seem to be of strictly regional interest to Middle Eastern economic geologists for copper/gold resource investigations in the arid and semi-arid regions.

***Acknowledgments*:** The authors are thankful to NASA Land Processes Distributed Active Archive Center User Services, USGS Earth Resources Observation and Science (EROS) Center (https://LPDAAC.usgs.gov) for providing the ASTER data. The authors would like to thank the ANJ Mine Exploration Company for providing borehole samples, in particular the Research and Development Department, for providing access to the area and logistical support. We are grateful to Aflak Mine Exploration Company for geological laboratory analyses. Authors are highly thankful to the Editor and anonymous reviewers of the journal for their valuable reviews and providing constructive comments and suggestions that have helped to present the work lucidly.

REFERENCES

Abdeen, M. M., Allison, T. K., Abdelsalam, M. G., & Stern, R. J. (2001): Application of ASTER band ratio images for geological mapping in arid regions; the Neoproterozoic Allaqi Suture, Egypt. *Geol. Soc. Am. Abstr, Programs* **3** (3), 289.

Aboelkhair, H., Ninomiya, Y., Watanabe, Y., & Sato, I. (2010): Processing and interpretation of ASTER TIR data for mapping of rare-metal-enriched albite granitoids in the Central Eastern Desert of Egypt. *Journal of African Earth Sciences*, **58** (1), 141–151.

Abrams, M., Hook, S., Ramachandran, B. (2002): *ASTER User Handbook*. Second ed. JPL Publication Laboratory, California Institute of Technology, 135.

Alimohammadi, M., Alirezaei, S., & Kontak, D. J. (2015): Application of ASTER data for exploration of porphyry copper deposits: A case study of Daraloo-Sarmeshk area, southern part of the Kerman copper belt, Iran. *Ore Geology Reviews*, **70**, 290–304.

Amer, R., El Mezayen, A., & Hasanein, M. (2016): ASTER spectral analysis for alteration minerals associated with gold mineralization. *Ore Geology Reviews*, **75**, 239–251.

Amer, R., Kusky, T., & El Mezayen, A. (2012): Remote sensing detection of gold related alteration zones in Um Rus area, Central Eastern Desert of Egypt. *Advances in Space Research*, **49** (1), 121–134.

Amer, R., Kusky, T., & Ghulam, A. (2010): Lithological mapping in the Central Eastern Desert of Egypt using ASTER data. *Journal of African Earth Sciences*, **56** (2), 75–82.

Austin, S. A. (1996): Excess argon within mineral concentrates from the new dacite lava dome at Mount St. Helens volcano. *Creation Ex Nihilo Technical Journal*, **10** (3), 335–343.

Azizi, H., Tarverdi, M., & Akbarpour, A. (2010): Extraction of hydrothermal alterations from ASTER SWIR data from east Zanjan, northern Iran. *Advances in Space Research*, **46** (1), 99–109.

Bachmann, O., & Bergantz, G. W. (2004): On the origin of crystal-poor rhyolites: extracted from batholithic crystal mushes. *Journal of Petrology*, **45** (8), 1565–1582.

Bedell, R. (2001): Geological mapping with ASTER satellite: new global satellite data that is a significant leap in remote sensing geologic and alteration mapping. *Special Publication Geology Society of Nevada*, **33**, 329–334.

Bedini, E. (2011): Mineral mapping in the Kap Simpson complex, central East Greenland, using HyMap and ASTER remote sensing data. *Advances in Space Research*, **47** (1), 60–73.

Clark, R. N., King, T. V., Klejwa, M., Swayze, G. A., & Vergo, N. (1990): High spectral resolution reflectance spectroscopy of minerals. *Journal of Geophysical Research: Solid Earth*, **95** (B8), 12653–12680.

Crosta, A., De Souza Filho, C., Azevedo, F., & Brodie, C. (2003): Targeting key alteration minerals in epithermal deposits in Patagonia, Argentina, using ASTER imagery and principal component analysis. *International Journal of Remote Sensing*, **24** (21), 4233–4240.

Cudahy, T., Jones, M., Thomas, M., Laukamp, C., Caccetta, M., Hewson, R., Roger, A. Verrall, M. (2008): Next generation mineral mapping: Queensland airborne HyMap and satellite ASTER surveys 2006–2008. CSIRO Exploration & Mining Report, P2007/2364.

Di Tommaso, I., & Rubinstein, N. (2007): Hydrothermal alteration mapping using ASTER data in the Infiernillo porphyry deposit, Argentina. *Ore Geology Reviews*, **32** (1), 275–290.

Gabr, S., Ghulam, A., & Kusky, T. (2010): Detecting areas of high-potential gold mineralization using ASTER data. *Ore Geology Reviews*, **38** (1), 59–69.

Gupta, R. P. (2003): *Remote Sensing Geology*. second ed. Springer, Heidelberg.

Hezarkhani, A. (2006): Hydrothermal evolution of the Sar-Cheshmeh porphyry Cu–Mo deposit, Iran: Evidence from fluid inclusions. *J. Asian Earth Sci*, **28**, 409–422.

Hunt, G. R. (1977): Spectral signatures of particulate minerals in the visible and near infrared. *Geophysics*, **42** (3), 501–513.

Hunt, G. R., & Ashley, R. P. (1979): Spectra of altered rocks in the visible and near infrared. *Economic Geology*, **74** (7), 1613–1629.

Ibrahim, W. S., Watanabe, K., & Yonezu, K. (2016): Structural and litho-tectonic controls on Neoproterozoic base metalsulfide and gold mineralization in North Hamisana shear zone, South Eastern Desert, Egypt: The integrated field, structural, Landsat 7 ETM + and ASTER data approach. *Ore Geology Reviews*, **79**, 62–77.

Khan, S. D., & Mahmoud, K. (2008): The application of remote sensing techniques to the study of ophiolites. *Earth-Science Reviews*, **89**, 135–143.

Kumar, C., Shetty, A., Raval, S., Ray, C., & Sharma, R. (2015): Lithological Discrimination and Mapping using ASTERSWIR Data in the Udaipur area of Rajasthan, *India. Procedia Earth and Planetary Science* **11**, 180–188.

Liu, F., Wu, X., Sun, H., & Guo, Y. (2007): Alteration information extraction by applying synthesis processing techniques to Landsat ETM+ data: case study of Zhaoyuan Gold Mines, Shandong Province, China. *Journal of China University of Geosciences*, **18** (1), 72–76.

Mars, J. C., & Rowan, L. C. (2006): Regional mapping of phyllic and argillic-altered rocks in the Zagros magmatic arc, Iran, using Advanced Spaceborne Thermal Emission and Reflection Radiometer (ASTER) data and logical operator algorithms. *Geosphere*, **2** (3), 161–186.

Modarres, R., & Da Silva, V. P. R. (2007): Rainfall trends in arid and semi-arid regions of Iran. *J. Arid Environ*, **70**, 344–355.

Moghtaderi, A., Moore, F., & Mohammadzadeh, A. (2007): The application of advanced space-borne thermal emission and reflection (ASTER) radiometer data in the detection of alteration in the Chadormalu paleocrater, Bafq region, Central Iran. *Journal of Asian Earth Sciences*, **30** (2), 238–252.

Ninomiya, N., Fu, B., & Cudahy, T. J. (2005): Detecting lithology with advanced spaceborne thermal and reflection radiometer (ASTER) multispectral thermal in frared "radiance-at-sensor" data. *Remote Sensing of Environment*, **99**, 127–135.

Ninomiya, Y. (2003): A stabilized vegetation index and several mineralogic indices defined for ASTER VNIR and SWIR data. *Geoscience and Remote Sensing Symposium, 2003*, IGARSS'03. *Proceedings*. IEEE International.

Pour, A. B., & Hashim, M. (2011): Identification of hydrothermal alteration minerals for exploring of porphyry copper deposit using ASTER data, SE Iran. *Journal of Asian Earth Sciences*, **42** (6), 1309–1323.

Pour, A. B., & Hashim, M. (2012a): The application of ASTER remote sensing data to porphyry copper and epithermal gold deposits. *Ore Geology Reviews*, 44, 1–9.

Pour, A. B., & Hashim, M. (2012b): Identifying areas of high economic-potential copper mineralization using ASTER data in the Urumieh–Dokhtar Volcanic Belt, Iran. *Advances in Space Research*, **49** (4), 753–769.

Rajendran, S., Nasir, S., Kusky, T. M., Ghulam, A., Gabr, S., & El-Ghali, M. A. (2013): Detection of hydrothermal mineralized zones associated with listwaenites in Central Oman using ASTER data. *Ore Geology Reviews*, 53, 470–488.

Regard, V., Bellier, O., Thomas, J. -C., Abbassi, M. R., Mercier, J., Shabanian, E., Feghhi. K.. Soleymani, S. (2004): Accommodation of Arabia–Eurasia convergence in the Zagros–Makran transfer zone, SE Iran: A transition between collision and subduction through a young deforming system. *Tectonics*, 23, 4, 24.

Rockwell, B. W., & Hofstra, A. H. (2008): Identification of quartz and carbonate minerals across northern Nevada using ASTER thermal infrared emissivity data – Implications for geologic mapping and mineral resource investigations in well-studied and frontier areas. *Geosphere*, **4** (1), 218–246.

Rowan, L. C., Mars, J. C., & Simpson, C. J. (2005): Lithologic mapping of the Mordor, NT, Australia ultramafic complex by using the Advanced Spaceborne Thermal Emission and Reflection Radiometer (ASTER). *Remote Sensing of Environment*, **99** (1), 105–126.

Shafiei, B., Haschke, M., & Shahabpour, J. (2009): Recycling of orogenic arc crusttriggers porphyry Cu mineralization

in Kerman Cenozoic arc rocks, southeastern Iran. *Minera. Depo*, 44, 265–283.

Streckeisen, A. (1979): Classification and nomenclature of volcanic rocks, lamprophyres, carbonatites and melilitic rocks: Recommendations and suggestions of the IUGS Subcommission on the Systematics of Igneous Rocks. *Geology*, **7** (7), 331–335.

Velosky, J. C., Stern, R. J., & Johnson, P. R. (2003): Geological control of massive sulfide mineralizationin the Neoproterozoic Wadi Bidah shear zone, southwestern Saudi Arabia, inferences from orbital remote sensing and field studies. *Precambrian Res*, **123** (2–4), 235–247.

Wang, Y., Fan, W., & Guo, F. (2003): Geochemistry of early Mesozoic potassium-rich diorites-granodiorites in southeastern Hunan Province, South China: petrogenesis and tectonic implications. *Geochemical Journal*, **37** (4), 427–448.

Yamaguchi, Y., & Naito, C. (2003): Spectral indices for lithologic discrimination and mapping by using the ASTER SWIR bands. *Int. J. Remote. Sens*. **24**, 22, 4311–4323.

Zhang, X., Pazner, M., & Duke, N. (2007): Lithologic and mineral information extraction for gold exploration using ASTER data in the south Chocolate Mountains (California). *ISPRS Journal of Photogrammetry and Remote Sensing*, **62** (4), 271–282.

Zoheir, B. (2011): Transpressional zones in ophiolitic mélange terraines: potential exploration targets for gold in the South Eastern Desert, Egypt. *Journal of Geochemical Exploration*, **111** (1), 23–38.

Zoheir, B., & Emam, A. (2012): Integrating geologic and satellite imagery data for high-resolution mapping and gold exploration targets in the South Eastern Desert, Egypt. *Journal of African Earth Sciences*, **66**, 22–34.

Zoheir, B., & Emam, A. (2014): Field and ASTER imagery data for the setting of gold mineralizationin Western Allaqi–Heiani belt, Egypt: A case study from the Haimurdeposit. *Journal of African Earth Sciences*, **99**, 150–164.

Р е з и м е

СПЕКТРАЛНА АНАЛИЗА АСТЕР НА КАРПИТЕ ВО КОИ ИМА АСОЦИЈАЦИИ НА ПОРФИРСКАТА БАКАРНО-МОЛИБДЕНСКА МИНЕРАЛИЗАЦИЈА

Hamid Sabbaghi[1], Ali Moradzadeh[1], Hooshang Asadi Haroni[2]

[1]*School of Mining Engineering, College of Engineering, University of Tehran, North Kargar St., Tehran, Iran, 14395-515*
[2]*Centre for Exploration Targeting, Australian Research Council Center of Excellence for Core to Crust Fluid Systems (CCFS), School of Earth and Environment, The University of Western Australia, Crawley, WA 6009*
h.sabbaghi@ut.ac.ir

Клучни зборови: порфирски бакар, АСТЕР, ПЦА, бранови сооднои, Зафарканд**.**

Ова проучување ја истражува примената на методите на обработка на спектралните слики во АСТЕР-податоци за картирање на карпите во кои има асоцијации на порфирска бакар-молибденска минерализација. Примената на далечинска детекција во одредбата на варијациите на површинската минералогија, структурните елементи и литолошки граници може да помогне во одредбата на таквите односи. Податоците од сигналите собрани од рефлексиониот радиометар (АСТЕР) се искористени за картирање на таквите карпи во областа Зафарканд. Областа на проучување е лоцирана во централниот сегмент на вулканскиот појас Урумие-Доктар во Иран. Урумие-Доктар е потенцијална зона за истражување на нови порфирски наоѓалишта на бакар. Односот на брановите должини, пресметките на брановите должини, композитите на лажни бои и техниките на анализа на главните компоненти се користени за одредување на различните литолошки асоцијации во областа. Овие методи покажале разликување на киселите магматски карпи од интермедијарните магматски карпи со употреба на инфрацрвени зраци со каратки бранови должини (СВИР) на АСТЕР во регионален размер. Резултатите се покажале како ефикасни во согласност со резултатите на теренските истражувања и рудни микроскопски испитувања, а се во согласност со геолошката карта. Како заклучок произлегува дека користените методи на обработка на слика можат да озбезбедат ефективен начин на добивање информации при откривање на можни локации на минерализации за порфирски бакар и епитермално злато пред започнување на детални и скапи истражувања на терен. Екстракцијата на спектралните информации од податоците АСТЕР може да продуцира разбирлива и точна информација во истражувањата на бакар и злато насекаде во светот, вклучувајќи ги и оние кои допрва треба да бидат откриени.